Effects of SSRIs on the spatial transcriptome of dorsal raphe serotonin neurons

Henningson C.[1], Mlost, J.[1], Pollak Dorocic I.[1]

[1]Science for Life Laboratory, Department of Biochemistry and Biophysics, Stockholm University, Sweden

Correspondence: iskra.pollak@scilifelab.se

Abstract

The serotonin system is the main therapeutic target for antidepressant drugs, most notably the selective serotonin reuptake inhibitors (SSRIs). SSRIs such as fluoxetine are routinely prescribed as a first-line treatment for depression, as well as for a range of comorbid conditions, however the drugs' mechanism is not well understood. In order to study the molecular and transcriptional effects of SSRI administration on their primary target serotonin neurons we performed spatial transcriptomics, a spatially resolved RNA-sequencing method in intact brain tissue. Mouse brain sections containing the dorsal raphe nucleus and surrounding midbrain structures were sequenced using Visium spatial gene expression platform (10X Genomics). We characterized six molecularly and spatially distinct serotonin subpopulations. Both acute and chronic fluoxetine treatment induces a large number of changes in gene expression in the dorsal raphe nucleus. The *Htr1a* gene is upregulated after acute, and downregulated after chronic treatment, consistent with previous studies showing that blocking of the serotonin transporter SERT has downstream effects on $5HT_{1a}$ autoreceptors. Gene enrichment and network analysis identified key pathways modulated by SSRI administration, including Ras, MAPK and cAMP signalling pathways as well as pathways involved in axonal guidance. We also describe opposing treatment-dependent transcriptional changes of neuropeptides thyrotropin-releasing hormone (*Trh*) and Prodynorphin (*Pdyn*) with specific spatial localization within the dorsal raphe nucleus, among others. Overall, our transcriptomic and in-situ hybridization analysis reveals spatial and cell-type specific heterogeneity in SSRI action within the dorsal raphe nucleus.

Introduction

Depression is a leading contributor to the global disability burden, with high lifetime prevalence, elevated risk of suicide, and a critically increasing incidence[1]. The serotonin system in the brain is the primary target of current widely-used antidepressant treatments, particularly the Selective Serotonin Reuptake Inhibitors (SSRIs). These drugs are routinely prescribed as a first-line treatment for depression and a range of comorbid conditions including anxiety and bipolar disorder, and are thus one of the most prescribed pharmaceutical drugs in the world. A large number of patients, in some countries as many as 10-15% of the total population[2], currently rely on antidepressants to alleviate their suffering, with SSRIs being the most common form of treatment[3]. SSRIs are generally efficacious and safe, nevertheless, these drugs still fail to alleviate depression in a significant portion of patients, have a slow onset and numerous side effects[4]. One of the challenges to developing better treatment strategies is the lack of understanding of SSRIs' mechanism of action.

Serotonin (5-hydroxytryptamine) is one of the major neuromodulators in the central nervous system, and plays a role in both normal function and disease. Serotonin interacts with at least 14 different receptor subtypes and therefore influences a wide range of physiological processes, from homeostatic maintenance to complex roles in mood and motivation[5]. All serotonin neurons in the mammalian brain are located in the collection of brainstem raphe nuclei, with the majority of forebrain-projecting serotonin neurons localised in the dorsal raphe nucleus (DR). Serotonin neurons within the DR are embedded in a wide neuronal network, receiving direct synaptic inputs from numerous forebrain regions[6–8], and subsequently projecting to a considerable number of brain areas where the release of serotonin has been linked to diverse behaviors[9].

One limitation of our current knowledge of the serotonin system, as well as its pharmacological targeting, is that the system has been considered unitary, *ie.* comprising all neurons that synthesize serotonin. Recently, however, several studies employing single-cell RNA sequencing have described the heterogeneity of the serotonin system and elucidated a number of molecular serotonergic subpopulations within the DR[10–12]. The DR cytoarchitecture is arranged in a broad-level topography, with neuron types spatially arranged in the dorsal, ventral and later DR sub-compartments and linked to distinct forebrain-circuits. Immunohistochemical labeling has shown topographical patterns of several different cell types within the DR, in addition to serotonin, the DR contains dopaminergic, glutamatergic and GABAergic neurons, as well as numerous neuropeptides[13,14]. The spatial expression of molecular markers in both serotonin and other cell types, as well as their overlap, may provide a clue to distinct functional roles of these subpopulations.

SSRIs exert their action by blocking the serotonin transporter (SERT). Blocking SERT increases extracellular serotonin concentration rapidly, within hours[15], however the clinical efficacy is only achieved with chronic use, usually several weeks[16]. This delay in effect is attributed to 5-HT_{1A} receptor desensitization. 5-HT_{1A} are Gi-coupled receptors that are expressed both post-synaptically but also as autoreceptors, hence they play an important role in providing feedback inhibition of serotonin neurons. Since SSRIs elevate synaptic serotonin levels, they also lead to activation of 5-HT_{1A} autoreceptor-driven feedback inhibition of serotonin neurons, causing a decrease in serotonin neuron firing and serotonin release[17,18]. Chronic SSRI treatment results in 5-HT_{1A} desensitization and loss of feedback inhibition, and serotonin neuron firing increases[19–21]. This influential hypothesis has been used to explain the delay in treatment effect, and to some extent the mechanism of action of SSRIs, however it has also been disputed[22], and several other mechanisms have been proposed, including downstream effects of enhanced hippocampal neurogenesis and increased synaptic plasticity[23]. Many questions remain about the effects of SSRI treatment on a molecular level.

Studies have shown that antidepressants can alter the expression of hundreds of genes in different brain regions, including the prefrontal cortex, hippocampus and amygdala[24–26]. However, these studies focused on a limited number of candidate genes and brain regions. Recently, a study utilized bulk RNA sequencing for unbiased profiling of a large number of brain regions of chronic fluoxetine treatment in the rat brain[27]. It showed that fluoxetine has a large effect on gene expression that varies substantially across brain regions, and the region where fluoxetine has the largest effect on the transcriptome is the raphe nucleus as a whole. Therefore, SSRIs produce large transcriptional effects on the main serotonergic nucleus, the raphe; however, the specific effects on serotonin neurons, their spatial subtypes, and other cell types in the DR are unknown.

Here, we performed spatial transcriptomics on the mouse midbrain, including the DR, in naïve healthy mice and in response to acute and chronic fluoxetine treatment. First, we describe the spatial transcriptional architecture of the DR, including single-cell resolution spatial characterization of novel markers that are co-expressed by DR serotonin neurons. Next, we analyse the transcriptional effects of SSRI treatment on these spatial serotonin subpopulations, and show differential treatment effects between acute and chronic administration, both spatially and on a single-cell level. Overall, our transcriptomic analysis reveals spatial and cell-type specific heterogeneity in SSRI action within the DR.

Results

Spatial transcriptomic profiling of midbrain and DR

Using unbiased and untargeted spatial transcriptomics, we profiled gene expression in coronal brain sections containing the DR and neighboring regions, in adult mice (**Fig. 1A**). We detected, on average, 3892 genes and 10,239 reads per spot (3892 ± 1133 unique genes, 10,239 ± 4978 reads). The complete dataset after quality control contained information on the expression of 30,413 unique genes across 8369 spots. Unsupervised UMAP clustering of gene expression across the whole brain section revealed 13 distinct clusters (**Fig. 1B**). We did not observe any batch nor sex mediated effects on clustering (**Fig. S1**). Aligning the molecular clusters with spatial location in brain tissue largely recapitulated anatomical brain regions, but also provided a higher-resolution delineation within the same brain region (**Fig. 1C**). For example, the periaqueductal gray (PAG) can be subdivided into the dorsal, lateral, ventrolateral and aqueductal PAG subregions with distinct molecular gene expression profiles. Spatial sequencing also clearly reveals the DR anatomical cluster, as well as a cluster flanking the DR bilaterally (**Fig. 1D**).

The DR cluster is clearly identified with the canonical serotonin markers, relating to serotonin synthesis, reuptake, release and regulation. These include: *Tph2* (Tryptophan hydroxylase 2), *Slc6a4* (serotonin transporter, SERT), *Slc18a2* (Vesicular monoamine transporter 2, VMAT2), *Ddc* (dopa decarboxylase), and *Gchfr* (GTP cyclohydrolase I feedback regulatory protein) that is involved in post-translational regulation of the serotonin synthesis pathway[28] (**Fig. 1E**). Another molecular cluster (lateral DR-GABA), flanks the DR bilaterally and is marked by *Gad2* expression. Overall, the spatial sequencing approach revealed molecular markers for midbrain anatomical structures, and reliably identified the DR based on serotonin-associated gene expression. The subsequent analysis focuses on the DR cluster, in order to define spatial subpopulations of serotonin neurons, and determine the effects of acute and chronic fluoxetine treatment.

Spatial subpopulations within DR serotonin system

The DR is a molecularly heterogeneous structure, containing different cell types. Several studies using single-cell RNA sequencing (scRNA-seq) have uncovered molecularly-

distinct serotonin subpopulations[10–12], however scRNA-seq does not retain spatial information. For this reason, some of these studies linked molecular serotonin subpopulations to spatial location using selected candidate genes uncovered by scRNA-seq. However, no fully unbiased way of linking transcriptomic profile directly to anatomical location in tissue has been performed in the DR.

Using spatial transcriptomics, we identified 6 molecular subclusters within the DR which largely correspond to spatial location and have distinct organization across the rostro-caudal axis (**Fig. 2A,B**). These clusters are defined by distinct gene profiles and display anatomical expression patterns, in particular we found a midline, ventral, caudal and two lateral clusters, as well as one non-serotonergic subcluster (**Fig. 2C**). All serotonergic clusters show strong molecular identity based on distinct marker genes, while the non-serotonergic cluster is defined by weak expression of canonical serotonin markers, likely containing less serotonin neurons compared to other DR spots. Some of the spatial marker genes are specific to the DR region, for example we found genes specific to the midline (*Slc17a8, Pdyn)*, caudal (*Met*) and one of the lateral clusters (*Wfdc12*, *Trh*) that are mostly restricted to the DR (**Fig. 2D**). Other prominent markers associated with the ventral (*Apod*) and second lateral (*Avp*, *Slc5a7*) cluster were not restricted to the DR, with an extended expression in the tissue section. Lateral cluster 2 shows distinct spatial and molecular expression compared to Lateral cluster 1, due to its proximal location to cholinergic neurons arising from the rostral lateral dorsal tegmental nucleus (expressing *Slc5a7*).

Based on spatial transcriptomics results, we selected several genes to analyse using multiplexed in-situ hybridization (ISH) in the DR, to reveal single-cell resolution expression patterns (**Fig. 2E, F**). The midline cluster is defined by the expression of *Slc17a8*, also known as VGLUT3. This neural subpopulation has been extensively characterized, as it contains serotonin neurons that co-express the vesicular glutamate transporter 3 and are able to co-release glutamate in several forebrain regions[29–31]. We found that approximately half of *Slc17a8* neurons in the DR express *Slc6a4* (SERT) (48.3% +/- 10.7% of *Slc17a8* cells express *Slc6a4*, mean ± SD, n = 1880 *Slc17a8* neurons, n = 5 mice) corresponding with previous studies[13]. The GABAergic gene *Gad2* is also extensively expressed in the DR and surrounding regions. A minority of DR *Gad2* also co-expressed *Slc6a4* (10.9% +/- 3.4% of *Gad2* cells express *Slc6a4*, n = 3342 *Gad2* neurons, n = 4 mice). The serotonin receptor $5HT_{1A}$ is expressed throughout the DR, and due to it being an autoreceptor, is to a large extent expressed on serotonin neurons, though not exclusively (79.0% +/- 7% of *Htr1a* cells express Slc6a4, n = 2116 *Htr1a* neurons, n = 5 mice).

We further analysed the expression of several other genes, which are not major DR cell types or markers, that were uncovered by the spatial transcriptomic sequencing. *Pdyn*, encoding the neuropeptide prodynorphin, is found in the DR midline and is extensively expressed in serotonin neurons (78.0% +/- 6% of *Pdyn* cells express *Slc6a4*, n = 827 *Pdyn* neurons, n = 5 mice). *Trh*, which codes for thyrotropin-releasing hormone, is localised to the caudal and ventral lateral wings of DR, and overlaps with serotonin neurons to a minor extent (37.5% +/- 16.8% of *Trh* cells express *Slc6a4*, n = 483 *Trh* neurons, n = 5 mice). *Bdnf*, encoding brain derived neurotrophic factor, has long been linked to the regulation of stress and development of mood disorders[32], is expressed mostly laterally and is largely not expressed in serotonin neurons (9.4% +/- 2.8% of *Bdnf* cells express *Slc6a4*, n = 1618 *Bdnf* neurons, n = 5 mice). *Vip*, encoding vasoactive intestinal peptide, is localised to the dorsal DR, along the aqueduct, and also shows minimal co-expression with serotonin neurons (3.2% +/- 3.2% of *Vip* cells express *Slc6a4*, n = 286 *Vip* neurons, n = 5 mice). To summarise the data, we produced a molecular map of the DR, showing the spatial location of each marker gene and co-expression with serotonin neurons (**Fig. S2**). These data reveal spatially segregated molecularly-defined subpopulations within the DR.

Effects of acute and chronic SSRI treatment on DR serotonin system

Serotonin neurons are the primary targets of SSRIs, which exert their action by directly blocking SERT. While studies using different levels of gene-expression analysis have investigated other brain regions that are targeted by serotonin circuits, little is known about how SSRIs alter the transcriptomic activity of the DR and serotonin neurons themselves. To answer that question, we performed spatial RNA sequencing on DR tissue sections from fluoxetine-treated brains. Since fluoxetine, and other SSRIs, are known to have a delayed effect of several weeks, we sought to capture the dynamic gene expression changes from acute to chronic administration.

Three treatment protocols using gavage administration were administered to healthy, naïve mice: acute (single dose fluoxetine, 10mg/kg), chronic (22 days daily administration, 10mg/kg), and control (single dose of saline) (n=3/treatment group) (**Fig. 3A**). We sought to administer a dose and treatment schedule comparable to clinical use in treatment of depression[33,34]. Our analysis identified a range of differentially expressed genes (DEGs) between the control, acute and chronic treatment protocols in both the whole midbrain tissue clusters (**Fig. S3A**) and the DR clusters. Looking specifically within the DR, acute and chronic SSRI administration resulted in DEGs enriched in several important signalling pathways, including: Ras, MAPK, cAMP and axon guidance pathways (**Fig. 3B, Fig. S3B**). Chronic fluoxetine administration correlates with an overall decrease in expression of most of the axonal guidance genes we analysed, most prominently *Plxnc1*, a gene that encodes a member of the plexin family, regulating axon guidance, cell motility and migration[35] (**Fig. 3C**). The Ras pathway gene *Raspgrp1*, that activates the Erk/MAP kinase cascade, shows an upregulation after chronic administration. The serotonin receptor $5HT_{1a}$ (via *Htr1a* expression) is upregulated after acute fluoxetine administration, and downregulated after chronic administration. This effect is consistent with previous studies showing that the SSRI block of SERT has downstream effects on $5HT_{1a}$ autoreceptors, with eventual desensitization. Correspondingly, we also observe that *Fos*, the immediate early transcription factor often used as a proxy for neural activity, is downregulated over chronic treatment (**Fig. 3C)**. Overall, many functional categories of genes are dynamically regulated by SSRI administration over the course of treatment duration (**Fig. 3D, Fig. S3C**).

We investigated how many of the DEGs are uniquely modulated in each treatment condition by analyzing the degree of overlap between the DEGs in control, acute and chronic fluoxetine administration condition (**Fig. 3E, F**). Of the total 232 DEGs found in the DR cluster, 192 are downregulated and 153 are upregulated in total, across different treatment conditions. Comparing the treatments, the number of downregulated DEGs in the acute vs chronic treatment is highest, while each treatment comparison shows a large number of unique upregulated DEGs. Interestingly, very few up- and down-regulated DEGs are shared between all three treatment conditions.

In order to find key factors among DEGs, we performed network analysis of protein-protein interactions and selected the top three up- or down-regulated genes (**Fig. 4**). Following acute SSRI treatment, *Bdnf* was the only hub gene detected but among the top three upregulated genes were *Bdnf, Pdyn* and *Rgs5*, whereas the top three downregulated genes were *Myl9, Nptx2* and *Adgrl4* (**Fig. 4A)**. Following chronic SSRI treatment, we found 7 hub genes: *Nras, Fos, Calb1, Rras, Fcer1g, Pdyn* and *Csf1r* (**Fig. 4B**). Among the top three upregulated genes were *Med1, Fcer1g, Csf1r*, whereas top three downregulated genes were *Pdyn, Nptx2* and *Fxyd5* (**Fig. 4B**). When comparing acute vs chronic SSRI treatment, we found 10 hub genes: *Fos, Met, Kit, Hcrt, Rbfox3, Trh, Ntrk1, Vip, Pdyn, Nkx2-2* (**Fig. 4C**). Among the top three upregulated genes were *Socs4, Bmp1* and *Bhlhe22*, whereas top three downregulated genes were *Vip, Tnnt1* and *Nkx6-1* (**Fig. 4C**). Interestingly, the two neuropeptide genes, *Pdyn* and *Trh*, show opposite dynamic regulation over the time course of SSRI treatment. *Pdyn* is upregulated after acute and downregulated after chronic treatment,

compared to the baseline. By contrast, *Trh* is initially downregulated, and then upregulated after the course of treatment (**Fig. 3D**).

In summary, we found many transcriptional changes in the DR over the time course of SSRI administration. Dynamic gene expression modulation on a single gene level was seen between all three treatment protocols. The largest number of changes were seen between the acute and chronic condition, both in up- and down-regulated DEGs, as well as network effects.

Dynamic gene expression changes of DR neuropeptides in acute and chronic SSRI treatment

Transcriptomic analysis revealed opposite modulation of *Pdyn* and *Trh* over SSRI treatment conditions. To confirm the transcriptomic results, we performed ISH on DR tissue after acute, chronic and control fluoxetine administration. Indeed, we found that acute administration resulted in both an increase in the number of *Pdyn*-expressing cells as well as total number of single *Pdyn* mRNA spots in the midline DR (**Fig. 5A**). Chronic treatment partially reversed upregulation of *Pdyn*-expressing cells and mRNA spots observed after acute treatment. However, when we specifically analysed *Pdyn* and *Slc6a4* co-expressing neurons, we did not observe a treatment effect. Analysing *Trh* expression with ISH also showed consistent results with the transcriptomic data. Chronic treatment resulted in both an increase in the number of *Trh*-expressing cells as well as total number of single *Trh* mRNA spots in the lateral DR (**Fig. 5B**). No change after acute treatment was observed, nor was there an effect on *Trh* and *Slc6a4* co-expressing neurons. Therefore, the changes in expression of these neuropeptides do not seem to be specific to serotonin neurons, rather to the expression of these neuropeptides in the DR as a whole.

The gene *Slc17a8*, aka VGLUT3, has been speculated to play a role in the treatment effect of SSRIs[36]. We sought to clarify whether the expression levels of *Slc17a8* on their own, or in combination with serotonin expression, are affected by SSRI treatment. No treatment effects were observed in either of the DR subpopulations associated with glutamate expression (**Fig. 5C)**. DR subpopulations expressing *Gad2*, *Htr1a*, Bdnf, and *Vip* also did not show any treatment effects at the mRNA level (**Fig. S4**).

Discussion

Here we present a spatio-molecular map of DR using unbiased spatial and transcriptomic analysis. We uncovered 6 molecular subpopulations within the DR, each displaying a distinct spatial distribution. Our data complement previous single-cell RNA-sequencing studies[10–12] and expand the knowledge of the topographical organization of the DR. Our sequencing data point to several specific markers for spatial DR targeting, including *Slc17a8* and *Pdyn* specific to the midline DR, *Met* specific for caudal DR, and *Wfdc12* and *Trh* for the lateral DR. These may be valuable candidates for genetic targeting of spatio-molecular serotonin subpopulations using transgenic and viral approaches. We further investigated the expression of several neuropeptides, as these are widely expressed in the DR and contribute to the molecular heterogeneity of the nucleus[14]. We found spatially distinct expression of *Pdyn*, *Trh*, and *Vip*, with varying levels of molecular overlap with serotonin neurons.

Further, we investigated how DR gene expression is modified by SSRI administration. Comparing the transcriptional effects of acute and chronic SSRI administration revealed a large number of gene expression effects. Gene enrichment and network analysis allowed us to identify some key pathways modulated by SSRI treatment. From among 232 DEGs in DR, between 10-12 genes could be annotated to Ras, MAPK and cAMP signalling pathways as well as the pathways involved in axonal guidance. Deficits in axonal guidance have been associated with SSRI use, particularly during development[37], and chronic treatment with fluoxetine impacts the morphology and reduces the density of serotonergic axons innervating

the PFC and hippocampus[38,39]. We show that chronic fluoxetine administration decreased the expression levels of the axonal guidance gene *Plxnc1,* among others. Interestingly, most of the key regulators of RAS pathways were indeed detected as hub genes in network analysis. Changes in hub as well as top regulated genes such as *Bdnf, Csf1r, Nras, Rras, Fos, Met, Kit, Myl9* and *Ntrk1* generally support the neurotrophic hypothesis regarding molecular mechanism of antidepressant drugs[40].

In addition to neurotrophic factors, we were able to detect interesting changes in neuropeptide expression, which may drive more direct behavioral effects of SSRIs. The *Pdyn* gene encodes the opioid peptide dynorphin, which binds to kappa opioid receptors (KOR), forming the KOR/dynorphin system. KOR is one of three opioid receptors which produces analgesia, however it differs from the mu- and delta-receptor subtypes, in that its activation results in dysphoria and prodepressive-like behaviors[41]. The *Pdyn* gene is highly expressed in limbic-related areas such as the amygdala, hippocampus, nucleus accumbens, hypothalamus, and more recently has been discovered to be co-expressed in a subpopulation of DR serotonin neurons[10–12]. KOR signalling has been studied in the context of stress-induced depressive symptoms in both humans and animal models, however most attention has been placed on its interaction with the dopaminergic system and its role in motivation and addiction. Less is known about the serotonin- dynorphin-KOR relationship and the neurobiology of mood. In the forced swim test (FST), a standard rodent behavioral assay for measuring behavioral coping related to a depressive-like state, disruption of KOR signalling (with antagonists or knock-down mice) resulted in less immobility, *ie.* decreased depression-like behavior[42]. Therefore, the initial findings in non-cell type specific studies point to a pro-depressive role of KOR signalling. Indeed, in our transcriptomic profiling, we show that *Pdyn* expression is increased after acute SSRI administration, and decreased after chronic administration. This initial increase may be correlated with the reported acute effects of SSRI treatment initiation, which can include increased anxiety and suicide risk[43,44].

The other neuropeptide-coding gene which showed dynamic regulation over SSRI treatment is *Trh*, with downregulation after acute and upregulation after chronic treatment. Thyrotropin-releasing hormone (TRH) is part of the hypothalamic–pituitary–thyroid neuroendocrine axis, where it is involved in stimulating the thyroid and release of hormones. However, TRH is also expressed in limbic areas, including the hippocampus, amygdala and the lateral DR. TRH acts through TRH receptor-1 and -2 (TRHR1 and TRHR2), which are also expressed in these limbic regions. It has been proposed that the local TRH in the cortico-limbic regions has cognitive and emotional functions, and may play a role in depression[45]. TRH-R1 KO mice and TRH-R2 KO mice exhibit depression-like and anxiety-like behaviors[46,47], while in the clinical population patients with depression have a blunted TRH response, and depression symptoms are associated with hypothyroidism[45]. It is not known whether TRH systems in different brain regions may have distinct roles in regulating depression. We show that chronic SSRI treatment results in upregulation of the *Trh* gene, suggesting a possible role of DR *Trh* being involved in alleviating symptoms of depression.

Our data also supports the $5HT_{1a}$ desensitization hypothesis, as we observe $5HT_{1a}$ upregulation with the acute treatment and downregulations after chronic treatment, consistent with $5HT_{1a}$ desensitization over time. In accordance, we also detected downregulation in *Fos* expression following chronic SSRI treatment that may suggest inhibition of the overall activity of serotonergic neurons.

In summary, our results expand the current knowledge of the spatial and molecular complexity of the DR, and SSRIs' effect on this important serotonergic hub in the brain. We provide supporting evidence for some of the dominant theories regarding the delayed therapeutic effect of SSRIs such as the neurotrophic and $5HT_{1a}$ desensitization hypothesis. However, we also discovered a novel neuropeptide-based SSRI mechanism that might explain both the initial worsening and following improvement in depressive symptoms, i.e.

changes in the expression of *Pdyn* and *Trh.* The candidate genes, pathways and cell types uncovered pave the way for deeper mechanistic studies to unravel the underpinnings of depression, and reveal novel targets for more specific pharmacological targeting.

Acknowledgements
This study was supported by SciLifeLab and Wenner Gren Foundations grants to I.P.D, and Polish National Agency for Academic Exchange (The Bekker Programme - BPN/BEK/2021/1/00152) and SciLifeLab RED Postdoctoral Fellowship to J.M. The authors acknowledge support from the National Genomics Infrastructure in Stockholm funded by Science for Life Laboratory, the Knut and Alice Wallenberg Foundation and the Swedish Research Council, and SNIC/Uppsala Multidisciplinary Center for Advanced Computational Science for assistance with massively parallel sequencing and access to the UPPMAX computational infrastructure. This work was supported by the National Bioinformatics Infrastructure Sweden (NBIS) at SciLifeLab. We thank Ana Rita Costa, and all the members of the Pollak Dorocic lab for thoughtful discussion, and C. Broberger for generous use of technical equipment.

Author contributions
C.H. performed the experiments, analysed and visualised the data. J.M. contributed to spatial transcriptomic analysis and produced the network analysis. I.P.D. conceived and supervised the study. All authors wrote and edited the manuscript.

Competing interests
The authors declare no competing interests.

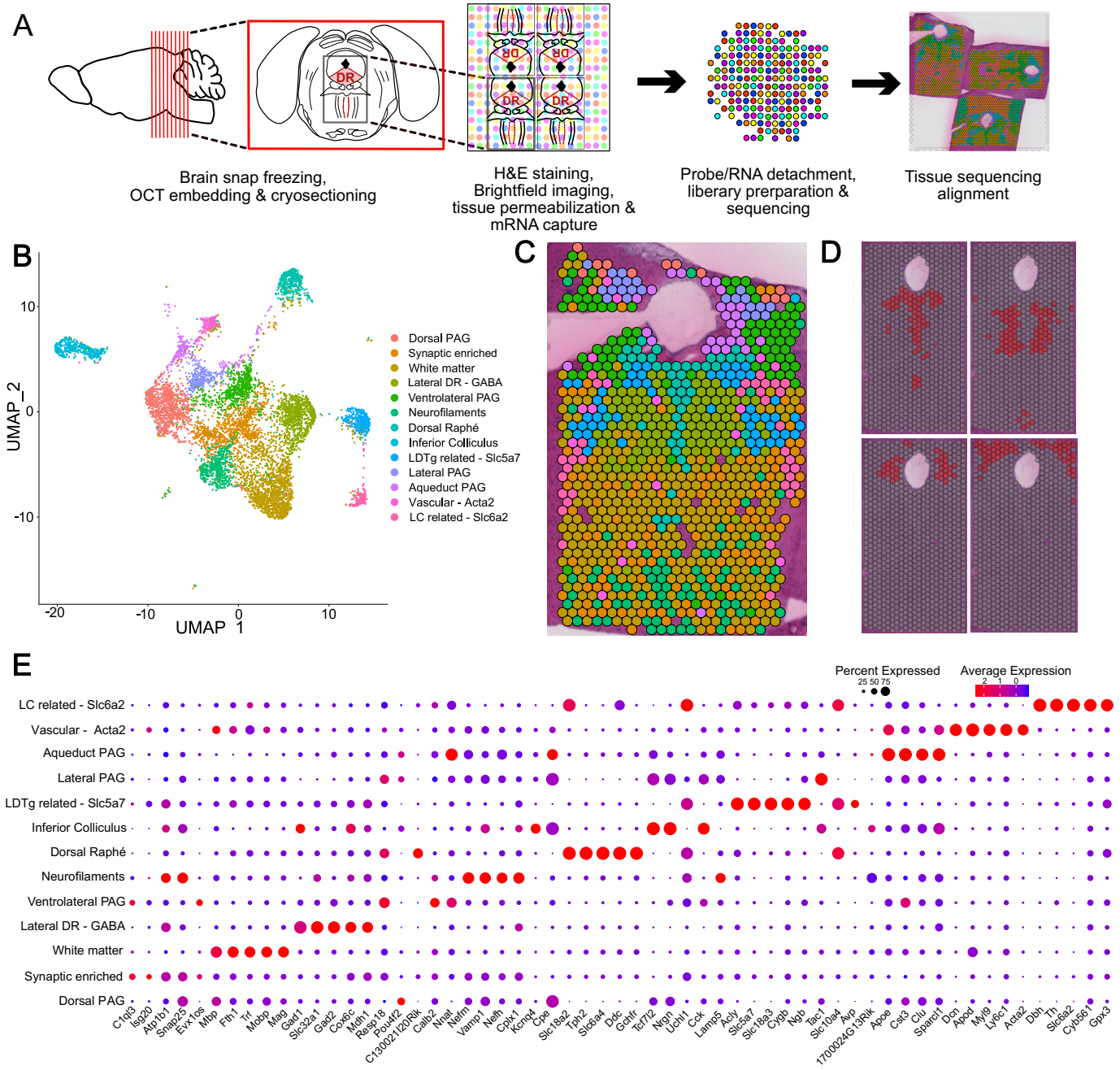

Figure 1. Spatial transcriptomic profiling of midbrain and DR

A. Experimental strategy: Coronal sections of mouse midbrain including the DR were cut and sections were mounted on Visium slide capture areas, followed by RNA sequencing and tissue alignment.

B. UMAP plot based on the transcriptional signature of each spot, covering the whole midbrain section, revealed 13 molecular clusters. Acronyms in cluster names: PAG, periaqueductal gray; DR, dorsal raphe; LDTg, laterodorsal tegmental nucleus; LC, locus coeruleus.

C. Representative midbrain tissue section with overlaid sequencing spots, color represents molecular cluster in (B).

D. Visualization of four anatomically distinct spatio-molecular clusters, including DR (top left), lateral DR (top right), lateral PAG (LPAG, bottom left) and dorsal PAG (bottom right).

E. Dot plot for each molecular cluster with expression level of individual genes. Diameter of the dot corresponds to the percentage of spots in the cluster expressing the gene, color indicates average expression of the gene.

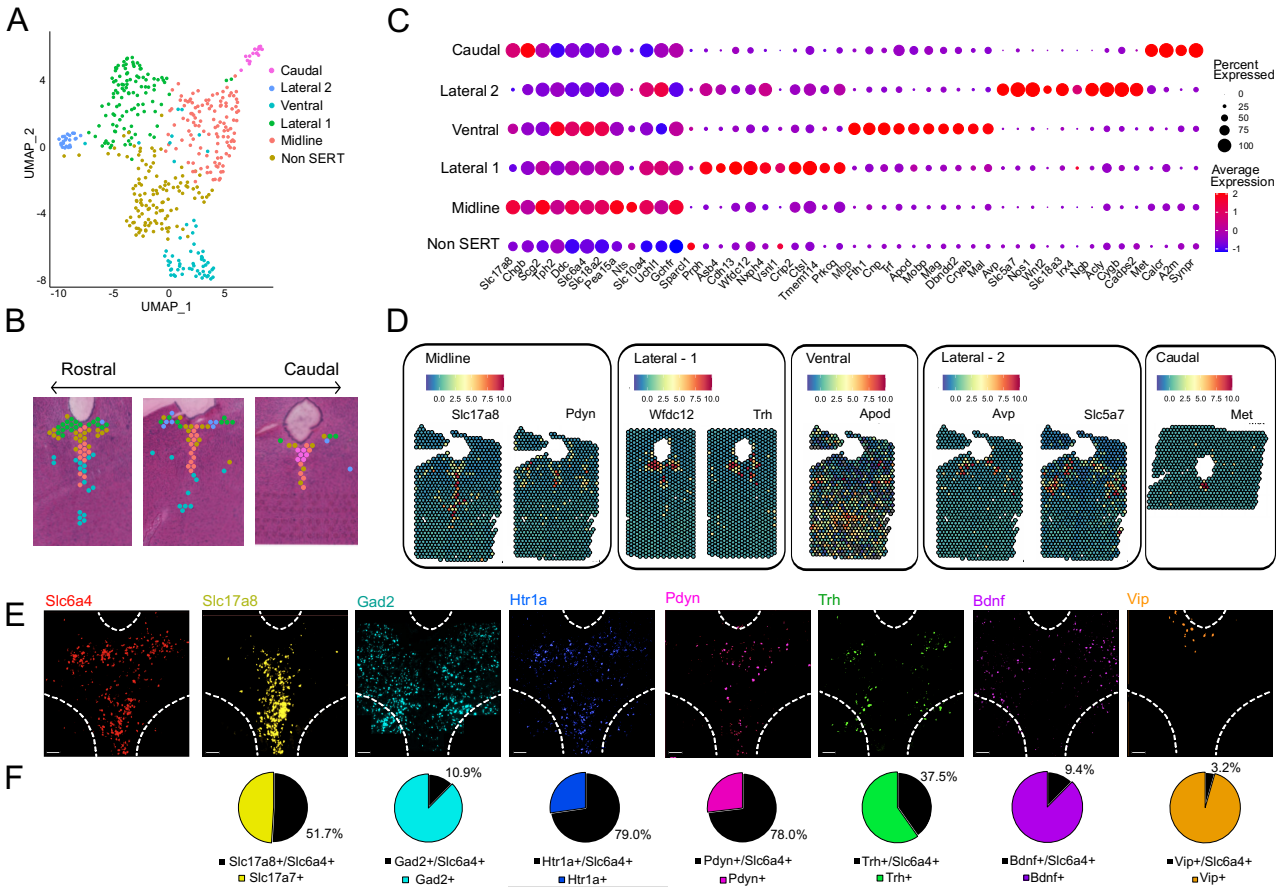

Figure 2. Spatio-molecular mapping of dorsal raphe nucleus

A. UMAP plot based on the transcriptional signature of each DR spot, cluster names refer to the spatial location or molecular identity.

B. Molecular clusters from A overlaid with tissue section, showing spatial localization of each cluster in DR and rosto-causal expression patterns.

C. Dot plot showing expression of 10 cluster marker genes per cluster. Diameter of the dot corresponds to the percentage of spots in the cluster expressing the gene, color indicates average expression of the gene.

D. Spatial heatmap of gene expression in DR for selected marker genes. Example of DR-specific markers (eg. midline-*Slc17a8*, *Pdyn*) and non-DR-specific marker genes (ventral-*Apod*).

E. In-situ hybridization in DR (area within broken white border) with 8 probes*: Slc6a4, Gad2, Slc17a8, Htr1a, Pdyn, Trh, Bdnf, Vip,* each displaying a distinct single-cell distribution pattern within DR.

F. Quantification of the co-expression of each marker gene from (E) with serotonin marker *Slc6a4* (SERT). Scale bar = 100µm.

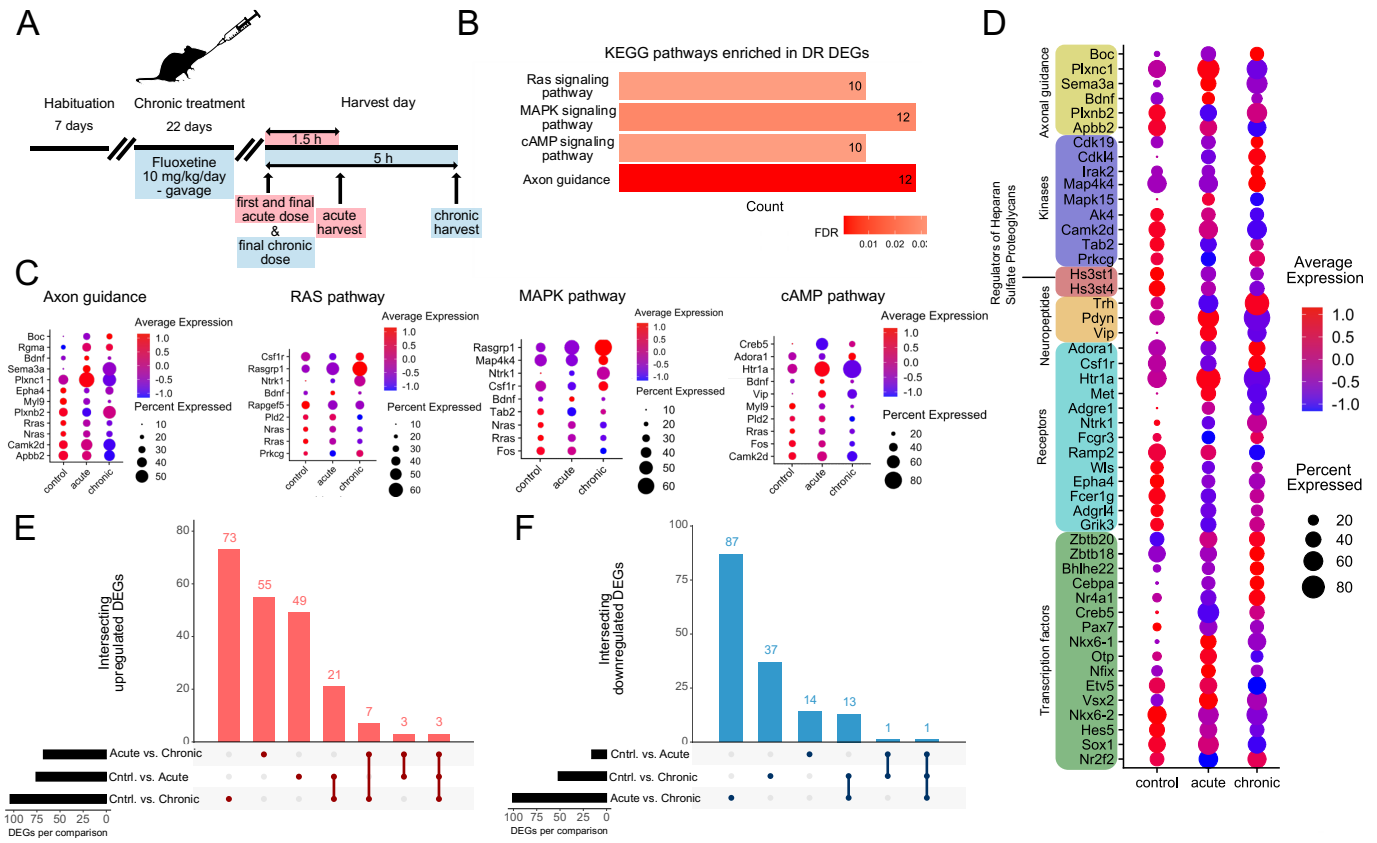

Figure 3. SSRI-induced gene expression changes in the DR

A. Schematic representation of the pharmacological experiment.

B. Gene enrichment analysis in the KEGG database of DEGs in the DR. Number in the bar represents the number DEGs observed across all treatment conditions.

C. Expression profiles of single DEGs in the DR, categorized by the involvement in specific KEGG pathways.

D. List of DEGs in the DR categorized by function from the Mouse Genome Informatics database and their expression levels across control, acute and chronic treatment conditions.

E. Upset plot of upregulated genes in the DR, between treatment conditions.

F. Upset plot of downregulated genes in the DR, between treatment conditions.

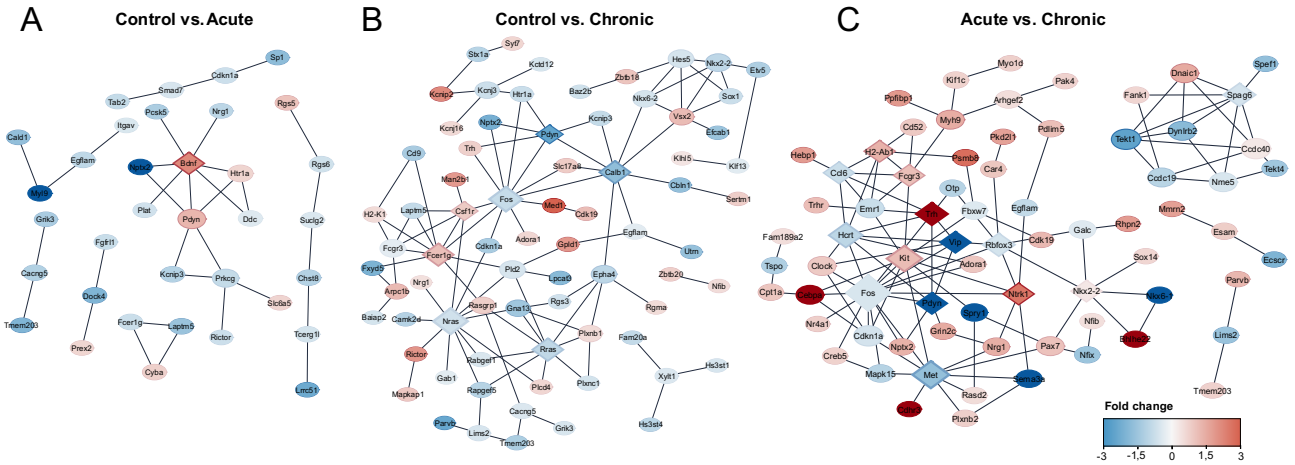

Figure 4. Network analysis of DEGs in DR

Based on the DEGs in DR, we have created a protein-protein interaction network in STRING database for changes in each comparison condition: control vs. acute (A), control vs. chronic (B) and acute vs. chronic (C). Hub genes are marked in a diamond node (◆). Red color denotes upregulation, whereas blue denotes downregulation in comparison to control (A-B) or acute (C) group.

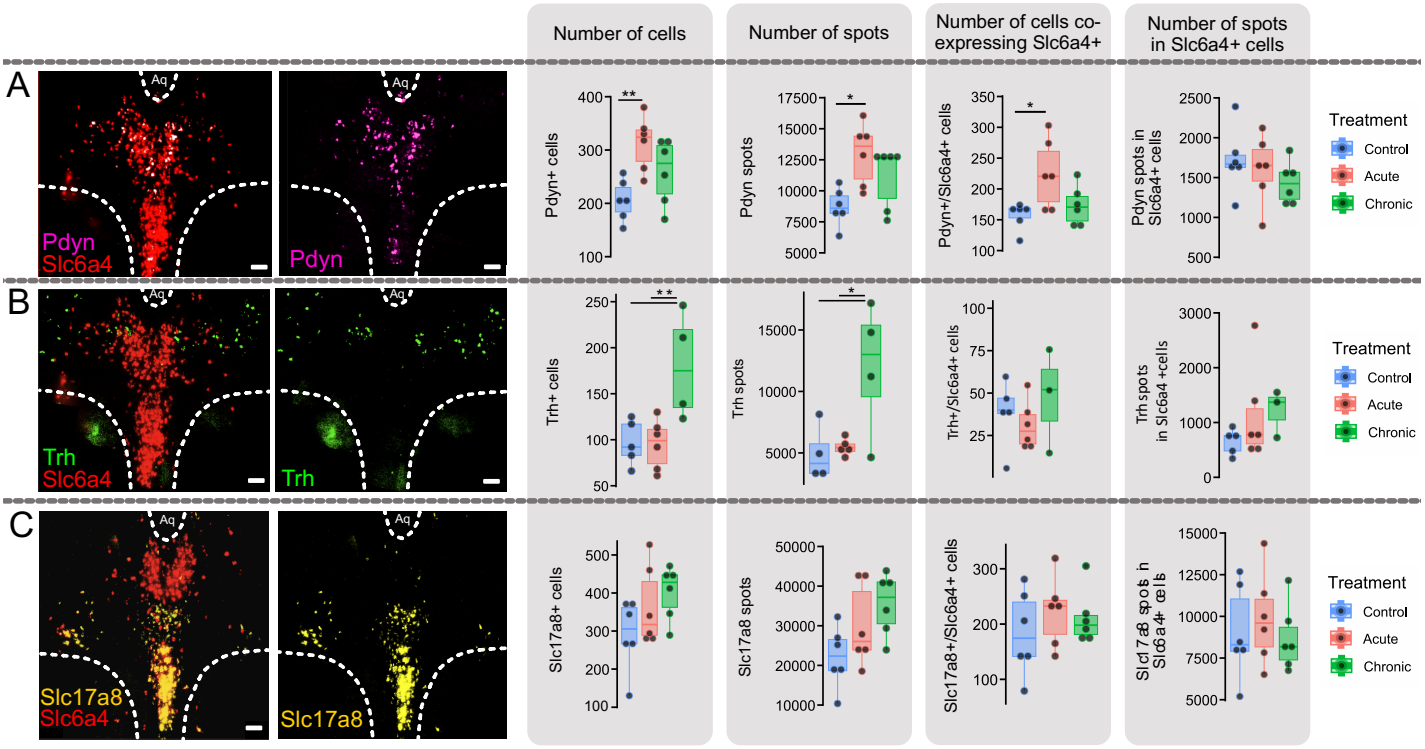

Figure 5. Dynamic gene expression changes of DR Pdyn, Trh and VGLUT3

A. Representative images of in-situ hybridization of *Pdyn* and *Slc6a4* co-expression and *Pdyn* in the DR. Box plots comparing treatment groups: sum of *Pdyn*+ cells per section (one-way ANOVA, $F(2,15) = 6.64$, $p = 0.009$**. Pairwise t-test with Holms correction; Acute vs Control, p=0.0072**), sum of *Pdyn* spots (transcripts) per section (one-way ANOVA, $F(2,15) = 5.735$, $p = 0.014$*. Pairwise t-test with Holms correction; Acute vs Control, p=0.0125*), sum of cells co-expressing *Pdyn* and *Slc6a4* per section (one-way ANOVA, $F(2,15) = 5.004$, $p = 0.022$*. Pairwise t-test with Holms correction; Acute vs Control, p=0.0255*), and sum of *Pdyn* spots in *Slc6a4* cells. Control n = 6, acute n=6, chronic n=6 mice per group.

B. Representative images of in-situ hybridization of Trh and Slc6a4 co-expression and Trh in the DR. Box plots comparing treatment groups of sum of Trh cells per section (one-way ANOVA, $F(2,12) = 7.684$, $p = 0.007$**. Pairwise t-test with Holms correction; Acute vs Chronic, $p = 0.0114$*; Chronic vs Control, p=0.0114*, control n = 5, acute n=6, chronic n=4 mice per group), sum of Trh spots (transcripts) per slice (one-way ANOVA, $F(2,10) = 5.887$, $p = 0.02$*. Pairwise t-test with Holms correction; Acute vs Chronic, $p = 0.0376$*; Chronic vs Control, p=0.0376*, control n = 5, acute n=6, chronic n=4 mice per group), sum of cells co-expressing Trh & Slc6a4 per section and sum of Trh spots in Slc6a4 + cells.

C. Representative images of in-situ hybridization of Slc17a8 and Slc6a4 co-expression and Slc17a8 in the DR. Box plots comparing treatment groups of sum of Slc17a8 cells per section, sum of Slc17a8 spots (transcripts) per slice, sum of cells co-expressing Slc17a8 & Slc6a4 per and sum of Slc17a8 spots in Slc6a4 + cells. Control n = 6, acute n=6, chronic n=6 mice per group.

Dots represent individual animals, p-values shown follow $p < 0.05$ = *, $p < 0.01$ = **, $p < 0.001$ = ***. Scale bar = 100µm.

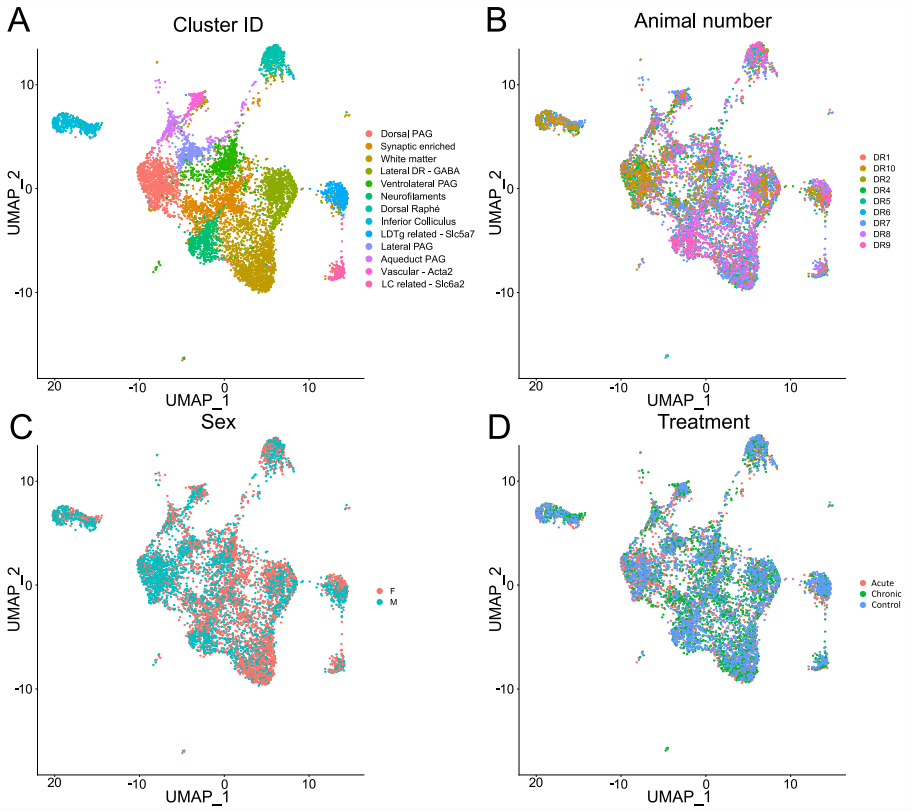

Figure S1. UMAP plot split by sample, sex, treatment
Lack of the technical- or batch- driven effects on clustering results in UMAP plot (**A**) was visualized by overlaying sample ID from different animals (**B**), their sex (**C**) or treatment group (**D**).

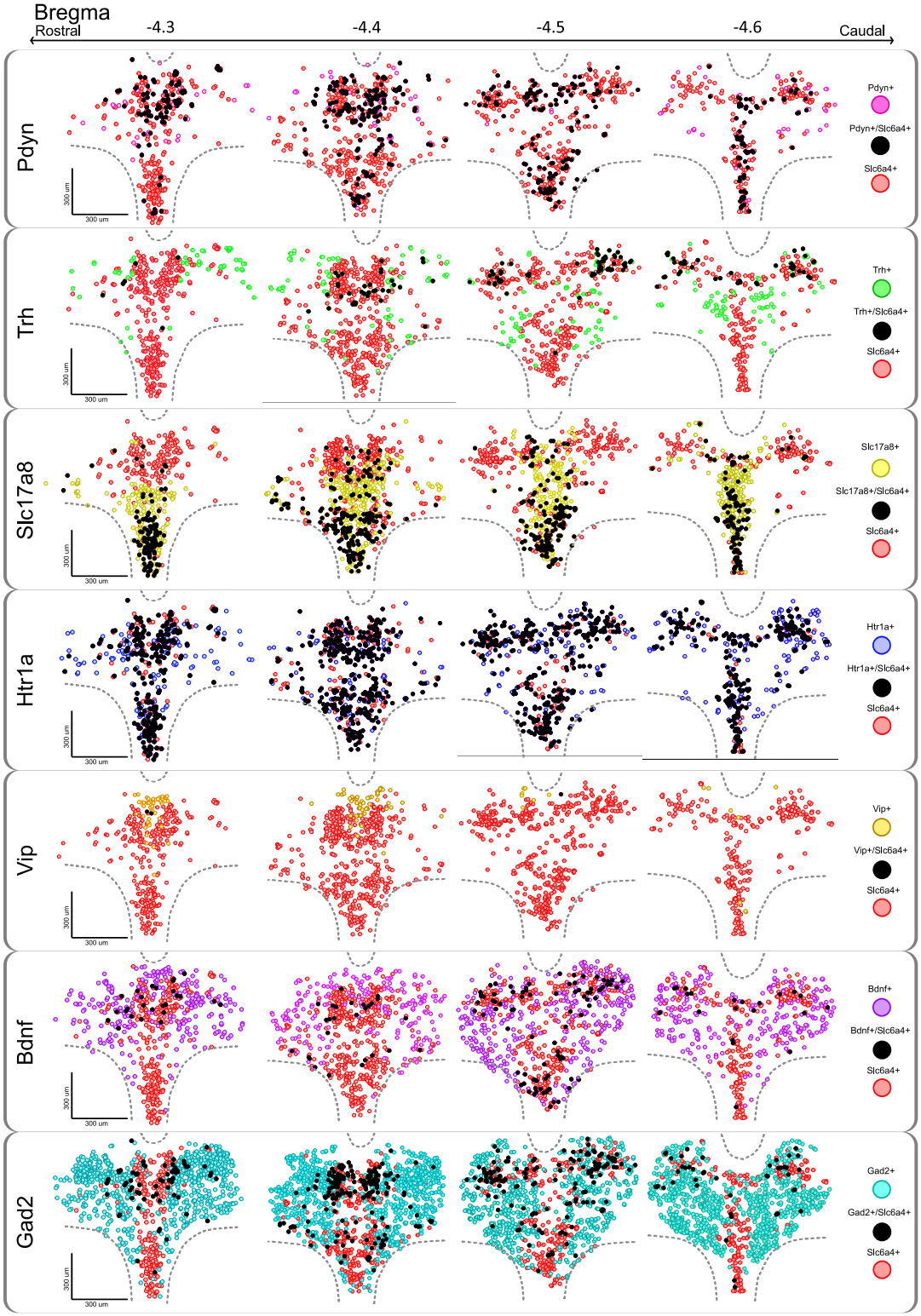

Figure S2. Spatio-molecular map of serotonin co-expression with other markers in DR
Expression of each marker gene (*Pdyn, Trh, Slc17a8, Htr1a, Vip, Bdnf, Gad2*) in the DR, along the rostro-caudal axis (4.3mm to -4.6mm). Co-expression of each specific marker with Slc6a4 (SERT) is marked by black circle (each circle correspond to a single cell), Slc6a4 positive cells lacking marker co-expression are marked in red, and the specific marker cells lacking Slc6a4 expression are shown in their respective color.

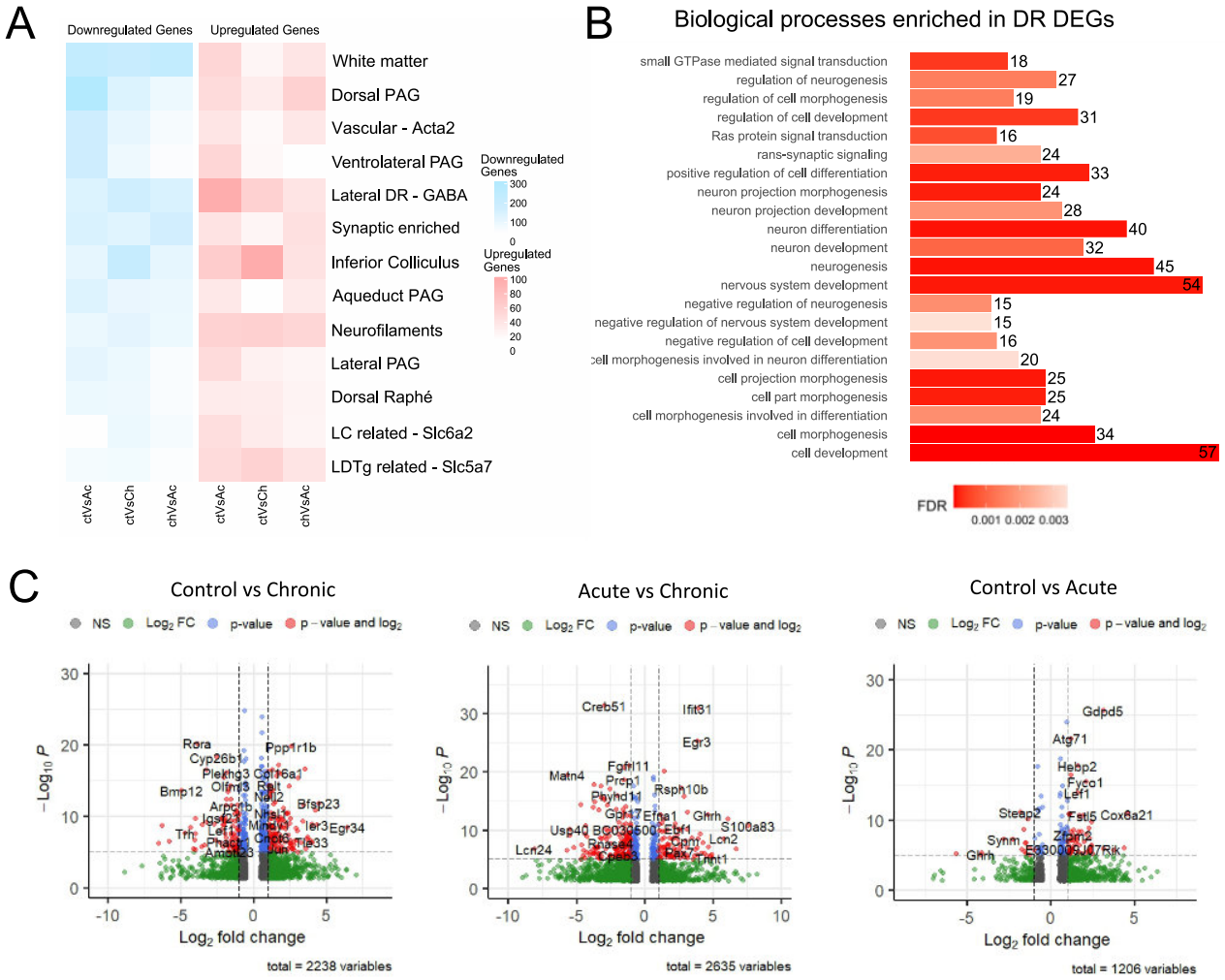

Figure S3. Differentially expressed genes in the midbrain and the DR

A. Heatmap visualization of the number of DEGs in midbrain's molecular clusters across different treatment conditions. The clusters correspond to UMAP in Fig. 1B.

B. Results of gene enrichment analysis in Gene Ontology, Biological Processes of DEGs in the DR across all treatment conditions.

C. Volcano plots representing top up- and down-regulated genes in the DR across different treatment conditions.

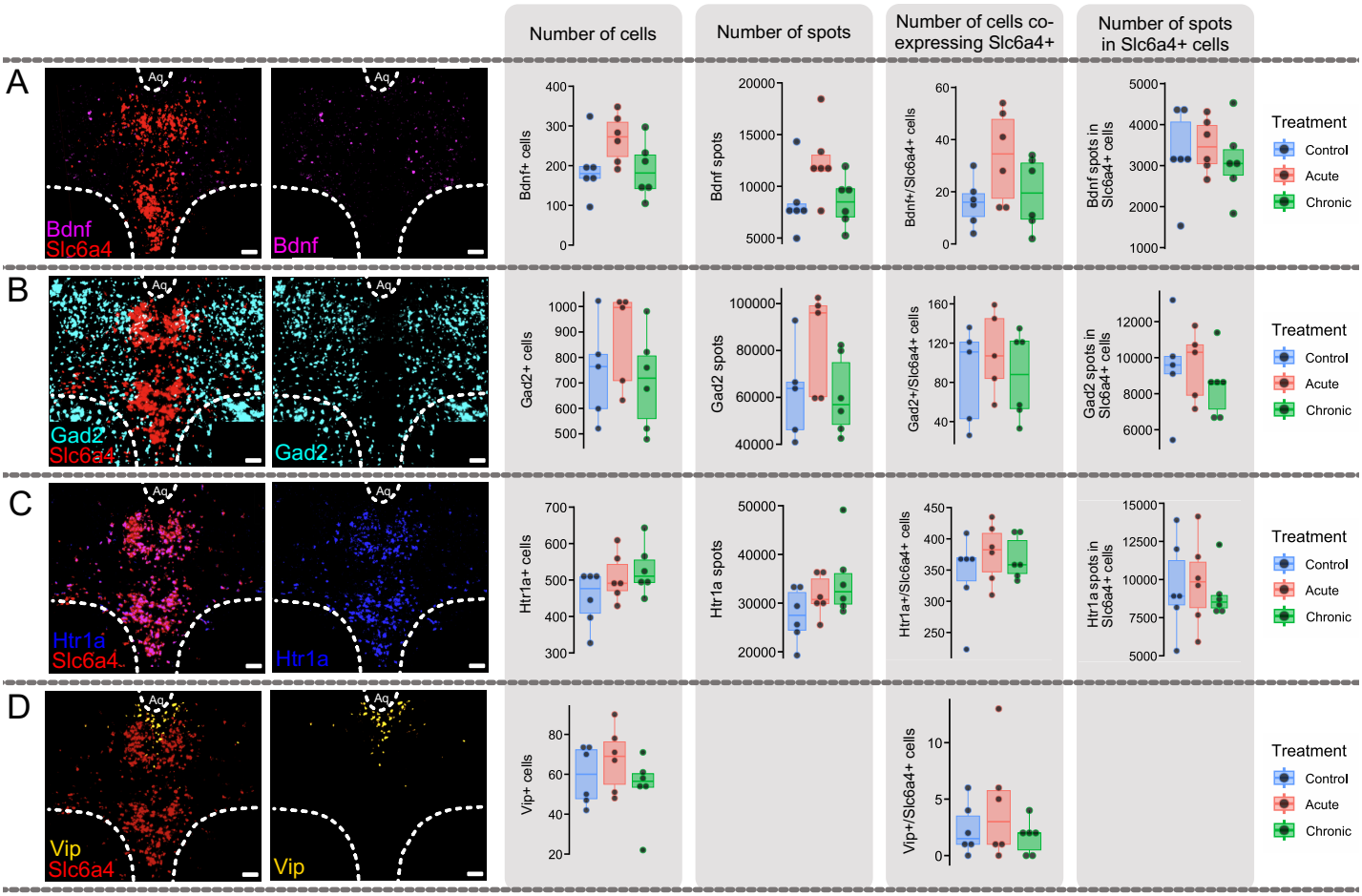

Figure S4. Gene expression of Bdnf, Gad2, Htr1a and Vip in the DR over SSRI treatment
A. Representative images of in-situ hybridization of *Bdnf* and *Slc6a4* co-expression and *Bdnf* in the DR. Box plots comparing treatment groups: sum of *Bdnf*+ cells per section, sum of *Bdnf* spots (transcripts) per section, sum of cells co-expressing *Bdnf* and *Slc6a4* per section, and sum of *Bdnf* spots in *Slc6a4* cells
B. Representative images of in-situ hybridization of *Gad2* and *Slc6a4* co-expression and *Gad2* in the DR. Box plots comparing treatment groups of sum of *Gad2*+ cells per section, sum of *Gad2* spots (transcripts) per, sum of cells co-expressing *Gad2* & *Slc6a4* per section and sum of *Gad2* spots in *Slc6a4*+ cells
C. Representative images of in-situ hybridization of *Htr1a* and *Slc6a4* co-expression and *Htr1a* in the DR. Box plots comparing treatment groups of sum of *Htr1a*+ cells per section, sum of *Htr1a* spots per slice, sum of cells co-expressing *Htr1a* & *Slc6a4* per and sum of *Htr1a* spots in *Slc6a4* + cells.
D. Representative images of in-situ hybridization of *Vip* and *Slc6a4* co-expression and *Vip* in the DR. Box plots comparing treatment groups of sum of *Vip*+ cells per section and sum of cells co-expressing *Vip* & *Slc6a4* per slice.
Scale bar = 100µm, control n = 6, acute n=6, chronic n=6 mice per group.

Methods

Animals

All experiments were carried out in adult C57BL/6J (Charles River) male and female mice. Mice were maintained under standard housing conditions with a 12-hour light cycle and with ad libitum access to food and water. All animal experiments had received approval from the local ethical board, Stockholms Norra Djurförsöksetiska Nämnd, and were performed in accordance with the European Communities Council Directive 2010/63. For spatial transcriptomics experiments, 9 mice (5 male, 4 female) were used, for *in-situ* hybridization 17 mice (9 females, 8 males) were used.

Fluoxetine administration

Fluoxetine Hydrochloride (Sigma-Aldrich, F132) was dissolved in saline and stored at -20C° until use. For administration the fluoxetine hydrochloride was diluted to 2 mg/ml and administered to the mice by gavage in 10 mg/kg dose. The dose was calculated to be within the range of human equivalent doses prescribed for depression. The standard dose of fluoxetine for treatment of depression in humans is 20mg/day, with the highest being 80 mg/day[1]. Assuming an adult human weighs 60kg,the range of doses are 0.333-1.333 mg/kg. converting the 10 mg/kg mouse dose into the human equivalent is 0.81 mg/kg[2].

The gavage procedure was performed with soft flexible feeding tubes to minimize the discomfort and potential damage to the animal. Mice in the acute treatment group received a single 10mg/kg dose of fluoxetine and brain tissue was harvested after 1,5h. Fluoxetine has been shown to produce behavioural effects in C57BL/6J mice after 30 min[3]. Mice in the chronic treatment group received 10 mg/kg/day for 22 consecutive days. The brain was harvested 5 h after the final dose to avoid any acute dose effect from the final dose. The control group received a single dose of saline instead at the equivalent volume to weight followed by brain harvest after 1.5 h.

Tissue preparation

Isoflourane was used to render the animals unresponsive before cervical dislocation. The animals were decapitated, the brain extracted and immediately placed in ice cold saline for a maximum of 15 sec. For spatial transcriptomics experiments, the midbrain was dissected on an ice cold metal block of approximately 5x5x2 mm. The brains utilized for RNAscope experiments remained whole. The tissue was flash frozen using powdered dry ice and was stored airtight at -80C° prior to sectioning. All tools and surfaces were cleaned with 70% ethanol and RNAase away (Thermo Scientific, 10666421) prior to and during the harvesting.

For spatial transcriptomics, the dissected midbrains were trimmed, labelled and embedded together in O.C.T. (VWR, 361603E). The blocks were sectioned on a cryostat in 10 µm coronal sections that were placed on the Visium slide capture areas. 3-4 trimmed brain sections were placed in single capture areas. For RNAscope experiments, whole brains were embedded in O.C.T., cut in 20 µm coronal sections on the cryostat and placed on SuperFrost+ slides and allowed to dry in the cryostat cold chamber. The slides were stored airtight at -80C° until either RNAscope or Visium experiment start.

Fluorescent in-situ hybridization

In situ hybridization to detect expression of genes of interest was performed using Hiplex RNAscope technology following the manufacturer's protocol for fresh frozen tissue (Advanced Cell Diagnostics, ACD, Hayward, CA). In brief, 20µm sections were fixed in 4% PFA (Sigma-Aldrich, 252549) solution (60 min, RT), dehydrated for 5 min each in 50%, 75%, 99% and 99% laboratory grade ethanol (Fisher Chemical E/0600DF/F17). The slides were stored overnight in 99% ethanol at -20C°. The next day the slides dried at RT and a hydrophobic barrier was drawn around each tissue section. Protease IV was added to permeabilize the

tissue sections (30 min, RT). After washing, each section was covered in probe dilution of 8 probes, or with positive and negative control probes, and incubated at 40C° for 2h in a humidity controlled environment. With wash steps between each incubation three amplification steps were performed, each 30 min 40C°. To reduce autofluorescence the slices were incubated with 3% FFPE reagent mix 30 min RT prior to 'HiPlex Fluoro T1–T4 v2', 15 min 40C°. After washing, DAPI staining was applied followed by clear mounting media and the first round of imaging.

The next day the sections were washed, and fresh cleaving solution was applied for 15 min RT two consecutive times, with washes in between to ensure removal of signal from previous imaging round. The slides were washed and incubated with 3% FFPE reagent mix 30 min RT, followed by 'HiPlex Fluoro T5–T8 v2 ' for 15 min 40C°. After washing, clear mounting media was added, followed by the second imaging round. The following probes were used: Htr1a-T1, Vip-T2, Bdnf-T3, Pdyn-T4, Trh-T5, Slc6a4-T6, Slc17a8-T7, Gad2-T8.

Microscopy

Imaging was performed on a Leica DM6 B stand up microscope with 40x oil immersion lens using the Leica developed LasX software. Intensities and exposure were setup on a separate tissue to minimize tissue bleaching. Each section was scanned in bright field and the image ROI was selected and saved. Several focus points were added for each ROI to ensure uniform focus throughout the stitched image. Each slice was imaged in 5 channels (DAPI, 488, 550, 650, 750) with a z-stack of 8x8 um depth over two separate imaging rounds. The LasX Mosaic Merge stitching tool was used to merge the individual images together, using the blend 'smooth' setting.

Image analysis

All images were imported to Fiji (ImageJ 2.14.0), using Bio-Formats importer to create a single max intensity projection image for all four channels (REF*4*). The max intensity image from imaging round 1 & 2 of the same slice was uploaded into a Qupath (0.5.0) project[4]. Using the Fiji/Qupath plugin, BigWarp in Fiji was utilized to create coordinate maps to overlap the two rounds of imaging based on the DAPI staining in the same slice.

Cell segmentation was performed in Qupath with Stardist scripts using their dsb2018_heavy_augment.pb model, identifying nuclei based in DAPI staining with 5.0 cell expansion and 0.5 threshold[5]. A region of interest was selected that included all Slc6a4+ cells, and corresponded with the Dorsal Raphe Nucleus location. Within this ROI Qupath's own 'Object Classification' was utilized to assign cell identity based on marker expression. Object classifiers were trained either on the image itself or on other images in the data set. Individual RNA puncta were quantified using Qupaths subcellular detection feature. The detection threshold was set individually for the image based on a combination of the autofluorescence of the image and the fluorescence strength seen in the negative control for the specific channel.

Objects and annotations and their measurements were transferred to the Round 2 image using the Warpy plugin "transfer annotations and measurements" .

Analysis & Statistics

The exported excel sheets for round 1 2 of imaging were imported in R. Using a custom R script, the total sum of puncta was summed per cell. Finally, the two rounds of exports were merged based on the shared cell object ID into a single data frame saved per animal and slice. All slices were combined into a larger data frame from which summary tables were produced to assess sum or cells, sum of spots, both per marker and co-expressing subpopulations. We tested our data for normal distribution and initially performed ANOVA to compare our three treatment groups, followed by pairwise t-test adjusted with the Holm-correction, if the ANOVA was statistically significant ($p<0.05$).

Spatial transcriptomics

The RNA integrity of the frozen tissue sections was measured with a bioanalyzer (Agilent) and was above 8 RIN for all samples. The 10x Genomics Visium protocol was performed by National Genomics Infrastructure at SciLifeLab, Sweden. Briefly, the sections were fixed with methanol at -20C° before performing H&E staining and bright field imaging. The tissue was then permeabilized enzymatically and the RNA was captured on the barcoded probes attached to the glass slide by the poly-A tail. The remaining tissue was washed away, and libraries were generated for each capture area and sequenced. Manual alignment of the H&E stained histology images to the expression spot grid was performed using the 10x Genomics Loupe Browser software (v. 5.1.0). The raw sequencing data files (FASTQ files) for the sequenced library samples were processed using the 10x Genomics Space Ranger software (v. 1.3.0) using the mouse genome reference transcriptome version GRCh38 2020-A (July 7, 2020) provided by 10x Genomics.

Analysis of Visium sequencing data

For each capture area the respective histological image was used for data alignment. The data was processed in R 4.2.2 with Seurat (V4.3.0).

Spots were filtered based on cutoff values on several QC parameters: spots containing less than 1000 genes, spots containing less than 1000 nFeatures, spots containing more than 24 % mitochondrial genes. Genes from a number of categories were removed from further analysis, which included haemoglobin genes, mitochondrial genes, ribosomal genes and X/Y chromosome genes. For each capture area, data was normalized using SCTransform with 'glmGamPoi' method, v2 vst.flavor and regressing out % mitochondrial genes and % ribosomal genes. Only a set of variable genes was returned for further analysis. In order to minimize batch effects, data across the capture areas was integrated using Reciprocal PCA based on top 3000 features and top 30 principal components. To find integration anchors we used capture area containing slices from the control-treated group as a reference and K = 10.

Clustering was performed using the original Louvain algorithm and resolution = 0.9. To visualize data points in two-dimensional space, we have performed Uniform Manifold Approximation and Projection (UMAP) on the first 20 principal components using 50 closest neighbours and spread = 2. Three clusters were excluded based on criteria that it must be present on a minimum two slices per condition. After initial clustering, we selected a cluster with elevated Tph2 expression as a DR cluster and subjected it to subclustering by using the same algorithms but changed the number of dimensions to top 8 and resolution to 0.8. We have carefully selected above mentioned algorithms and parameters by comparing clustering stability, purity and silhouette width. To find markers and perform differential gene expression analysis, we used FindMarkers() function on "data" slot from integrated dataset and compared medians by Wilcoxon Rank Sum test. We have set "logfc" threshold to 0.5 and minimum expression in at least 20% of cluster's spots. Differential gene expression was analysed comparing a single cluster with the rest of the dataset to find cluster marker genes and within the same cluster between treatment conditions to find treatment affected genes. For multiple comparison correction, we used False Discovery Rate and only changes with p-value < 0.05 were considered significant.

Network analysis: To identify key genes in DR affected by SSRI treatment, we created a Protein–Protein Interaction (PPI) Network with the STRING database using the list of all DEGs detected in DR, with significance cutoff value of FDR < 0.05 and minimum expression in at least 20% of the cluster spots. Network was then visualized and analyzed in Cytoscape (3.10.0). Based on the degree distribution in all three networks, the degree threshold value for hub genes was set to 6.

Gene enrichment analysis: In order to investigate the potential functional effects of the SSRI treatment in the DR we performed gene enrichment analysis through The Database for

Annotation, Visualization and Integrated Discovery (DAVID)[6,7] bioinformatics. We uploaded all DEGs detected in the DR, with significance cutoff value of FDR < 0.05 and minimum expression in at least 20% of the cluster spot, as a list in the DAVID analysis wizard and selected annotation categories KEGG pathways and GO terms Biological processes_5.

Reproducibility and sample size

Sample size based on other previous research with no calculations done prior to the experiments. All experiments contained between 3-6 biological replicates per group. Data was excluded based on raw data quality, if dissection of the slices did not contain the same clusters in all treatment groups, or if the cluster contained too few data points for further analysis.

References for methods:

1. Altamura, A. C., Moro, A. R. & Percudani, M. Clinical Pharmacokinetics of Fluoxetine. *Clin. Pharmacokinet.* **26**, 201–214 (1994).

2. Nair, A. B. & Jacob, S. A simple practice guide for dose conversion between animals and human. *J Basic Clin Pharm* **7**, 27–31 (2016).

3. Zl, J. *et al.* Mouse strain differences in SSRI sensitivity correlate with serotonin transporter binding and function. *Scientific reports* **7**, (2017).

4. Bankhead, P. *et al.* QuPath: Open source software for digital pathology image analysis. *Sci Rep* **7**, 16878 (2017).

5. Stevens, M. *et al.* StarDist Image Segmentation Improves Circulating Tumor Cell Detection. *Cancers (Basel)* **14**, 2916 (2022).

6. Sherman, B. T. *et al.* DAVID: a web server for functional enrichment analysis and functional annotation of gene lists (2021 update). *Nucleic Acids Res* **50**, W216–W221 (2022).

7. Huang, D. W., Sherman, B. T. & Lempicki, R. A. Systematic and integrative analysis of large gene lists using DAVID bioinformatics resources. *Nat Protoc* **4**, 44–57 (2009).

References

1. Moreno-Agostino, D. *et al.* Global trends in the prevalence and incidence of depression:a systematic review and meta-analysis. *Journal of Affective Disorders* **281**, 235–243 (2021).

2. OECD. *Pharmaceutical Market*. https://www.oecd-ilibrary.org/content/data/data-00545-en (2016).

3. Luo, Y., Kataoka, Y., Ostinelli, E. G., Cipriani, A. & Furukawa, T. A. National Prescription Patterns of Antidepressants in the Treatment of Adults With Major Depression in the US Between 1996 and 2015: A Population Representative Survey Based Analysis. *Frontiers in Psychiatry* **11**, (2020).

4. Ferguson, J. M. SSRI Antidepressant Medications: Adverse Effects and Tolerability. (2001).

5. Cools, R., Roberts, A. C. & Robbins, T. W. Serotoninergic regulation of emotional and behavioural control processes. *Trends Cogn Sci* **12**, 31–40 (2008).

6. Pollak Dorocic, I. *et al.* A Whole-Brain Atlas of Inputs to Serotonergic Neurons of the Dorsal and Median Raphe Nuclei. *Neuron* **83**, 663–678 (2014).

7. Weissbourd, B. *et al.* Presynaptic Partners of Dorsal Raphe Serotonergic and GABAergic Neurons. *Neuron* **83**, 645–662 (2014).

8. Ogawa, S. K., Cohen, J. Y., Hwang, D., Uchida, N. & Watabe-Uchida, M. Organization of monosynaptic inputs to the serotonin and dopamine neuromodulatory systems. *Cell Rep* **8**, 1105–1118 (2014).

9. Muzerelle, A., Scotto-Lomassese, S., Bernard, J. F., Soiza-Reilly, M. & Gaspar, P. Conditional anterograde tracing reveals distinct targeting of individual serotonin cell groups (B5–B9) to the forebrain and brainstem. *Brain Struct Funct* **221**, 535–561 (2016).

10. Ren, J. *et al.* Single-cell transcriptomes and whole-brain projections of serotonin neurons in the mouse dorsal and median raphe nuclei. *eLife* **8**, e49424 (2019).

11. Huang, K. W. *et al.* Molecular and anatomical organization of the dorsal raphe nucleus. *eLife* **8**, e46464 (2019).

12. Okaty, B. W. *et al.* A single-cell transcriptomic and anatomic atlas of mouse dorsal raphe Pet1 neurons. *eLife* **9**, e55523 (2020).

13. Cardozo Pinto, D. F. *et al.* Characterization of transgenic mouse models targeting neuromodulatory systems reveals organizational principles of the dorsal raphe. *Nat Commun* **10**, 4633 (2019).

14. Fu, W. *et al.* Chemical neuroanatomy of the dorsal raphe nucleus and adjacent structures of the mouse brain. *Journal of Comparative Neurology* **518**, 3464–3494 (2010).

15. Hervás, I. & Artigas, F. Effect of fluoxetine on extracellular 5-hydroxytryptamine in rat brain. Role of 5-HT autoreceptors. *Eur J Pharmacol* **358**, 9–18 (1998).

16. Stahl, S. M. Mechanism of action of serotonin selective reuptake inhibitors: Serotonin receptors and pathways mediate therapeutic effects and side effects. *Journal of Affective Disorders* **51**, 215–235 (1998).

17. Czachura, J. F. & Rasmussen, K. Effects of acute and chronic administration of fluoxetine on the activity of serotonergic neurons in the dorsal raphe nucleus of the rat. *Naunyn-Schmied Arch Pharmacol* **362**, 266–275 (2000).

18. Kreiss, D. S. & Lucki, I. Effects of acute and repeated administration of antidepressant drugs on extracellular levels of 5-hydroxytryptamine measured in vivo. *J Pharmacol Exp Ther* **274**, 866–876 (1995).

19. Hensler, J. Differential regulation of 5-HT1A receptor-G protein interactions in brain following chronic antidepressant administration. *Neuropsychopharmacology : official publication of the American College of Neuropsychopharmacology* **26**, (2002).

20. Artigas, F., Romero, L., de Montigny, C. & Blier, P. Acceleration of the effect of selected antidepressant drugs in major depression by 5-HT1A antagonists. *Trends in Neurosciences* **19**, 378–383 (1996).

21. de Montigny, C. & Blier, P. Effects of antidepressant treatments on 5-HT neurotransmission: electrophysiological and clinical studies. *Adv Biochem Psychopharmacol* **39**, 223–239 (1984).

22. Commons, K. G. & Linnros, S. E. Delayed Antidepressant Efficacy and the Desensitization Hypothesis. *ACS Chem Neurosci* **10**, 3048–3052 (2019).

23. Harmer, C. J., Duman, R. S. & Cowen, P. J. How do antidepressants work? New perspectives for refining future treatment approaches. *The Lancet Psychiatry* **4**, 409–418 (2017).

24. Carrillo-Roa, T. *et al.* Common genes associated with antidepressant response in mouse and man identify key role of glucocorticoid receptor sensitivity. *PLOS Biology* **15**, e2002690 (2017).

25. Conti, B. *et al.* Region-specific transcriptional changes following the three antidepressant treatments electro convulsive therapy, sleep deprivation and fluoxetine. *Mol Psychiatry* **12**, 167–189 (2007).

26. Surget, A. *et al.* Corticolimbic Transcriptome Changes are State-Dependent and Region-Specific in a Rodent Model of Depression and of Antidepressant Reversal. *Neuropsychopharmacol* **34**, 1363–1380 (2009).

27. Rayan, N. A. *et al.* Integrative multi-omics landscape of fluoxetine action across 27 brain regions reveals global increase in energy metabolism and region-specific chromatin remodelling. *Mol Psychiatry* 1–16 (2022) doi:10.1038/s41380-022-01725-1.

28. Wyler, S. C., Donovan, L. J., Yeager, M. & Deneris, E. Pet-1 Controls Tetrahydrobiopterin Pathway and Slc22a3 Transporter Genes in Serotonin Neurons. *ACS Chem. Neurosci.* **6**, 1198–1205 (2015).

29. Gras, C. *et al.* A Third Vesicular Glutamate Transporter Expressed by Cholinergic and Serotoninergic Neurons. *J. Neurosci.* **22**, 5442–5451 (2002).
30. Liu, Z. *et al.* Dorsal Raphe Neurons Signal Reward through 5-HT and Glutamate. *Neuron* **81**, 1360–1374 (2014).

31. Sengupta, A., Bocchio, M., Bannerman, D. M., Sharp, T. & Capogna, M. Control of Amygdala Circuits by 5-HT Neurons via 5-HT and Glutamate Cotransmission. *J. Neurosci.* **37**, 1785–1796 (2017).

32. Cavaleri, D. *et al.* The role of BDNF in major depressive disorder, related clinical features, and antidepressant treatment: Insight from meta-analyses. *Neuroscience & Biobehavioral Reviews* **149**, 105159 (2023).

33. Altamura, A. C., Moro, A. R. & Percudani, M. Clinical Pharmacokinetics of Fluoxetine. *Clin. Pharmacokinet.* **26**, 201–214 (1994).

34. Nair, A. B. & Jacob, S. A simple practice guide for dose conversion between animals and human. *J Basic Clin Pharm* **7**, 27–31 (2016).

35. Yuasa-Kawada, J., Kinoshita-Kawada, M., Tsuboi, Y. & Wu, J. Y. Neuronal guidance genes in health and diseases. *Protein & Cell* **14**, 238–261 (2023).

36. Fischer, A. G., Jocham, G. & Ullsperger, M. Dual serotonergic signals: a key to understanding paradoxical effects? *Trends in Cognitive Sciences* **19**, 21–26 (2015).

37. Homberg, J. R., Schubert, D. & Gaspar, P. New perspectives on the neurodevelopmental effects of SSRIs. *Trends in Pharmacological Sciences* **31**, 60–65 (2010).

38. Nazzi, S. *et al.* Reversible Morphological Remodeling of Prefrontal and Hippocampal Serotonergic Fibers by Fluoxetine. *ACS Chem. Neurosci.* **15**, 1702–1711 (2024).

39. Nazzi, S., Maddaloni, G., Pratelli, M. & Pasqualetti, M. Fluoxetine Induces Morphological Rearrangements of Serotonergic Fibers in the Hippocampus. *ACS Chem. Neurosci.* **10**, 3218–3224 (2019).

40. Casarotto, P. C. *et al.* Antidepressant drugs act by directly binding to TRKB neurotrophin receptors. *Cell* **184**, 1299-1313.e19 (2021).

41. Knoll, A. T. & Carlezon, W. A. Dynorphin, stress, and depression. *Brain Research* **1314**, 56–73 (2010).

42. McLaughlin, J. P., Marton-Popovici, M. & Chavkin, C. κ Opioid Receptor Antagonism and Prodynorphin Gene Disruption Block Stress-Induced Behavioral Responses. *J. Neurosci.* **23**, 5674–5683 (2003).

43. Ramos, R. T., Gentil, V. & Gorenstein, C. Clomipramine and initial worsening in panic disorder: beyond the 'jitteriness syndrome'. *J Psychopharmacol* **7**, 265–269 (1993).

44. Grillon, C., Levenson, J. & Pine, D. S. A Single Dose of the Selective Serotonin Reuptake Inhibitor Citalopram Exacerbates Anxiety in Humans: A Fear-Potentiated Startle Study. *Neuropsychopharmacol* **32**, 225–231 (2007).

45. Joffe, R. T. & Marriott, M. Thyroid Hormone Levels and Recurrence of Major Depression. *AJP* **157**, 1689–1691 (2000).

46. Zeng, H. *et al.* Thyrotropin-Releasing Hormone Receptor 1-Deficient Mice Display Increased Depression and Anxiety-Like Behavior. *Molecular Endocrinology* **21**, 2795–2804 (2007).